

**Military Technical College
Kobry El-Kobbah,
Cairo, Egypt.**



**13th International Conference
on Applied Mechanics and
Mechanical Engineering.**

SIMULATION OF A REVERSE OSMOSIS SEAWATER DESALINATION PLANT, PART 2: EXPERIMENTAL MEASUREMENTS AND PREDICTION STUDY ON THE VALIDATED SIMULATION MODEL

SEOUDY*A., LOTFY* A.H. and SALEH* I.

ABSTRACT

The present work introduces experimental investigations of a real reverse osmosis (RO) plant. Flowrate and pressure measurements have been performed. The pump pressure fluctuations at different flowrates and the permeate pressure of RO membrane at different seawater salinities have been measured experimentally. The results of the present experimental measurements and some of the previously published experimental results of RO membrane have been compared with the corresponding theoretical results of the plant theoretical model in order to validate the simulation program (presented in part 1 of this paper). In the present work the validated simulation model has been used to carry out prediction study to investigate the dynamic characteristics of the plant axial piston pump and the RO membrane performance under normal and abnormal operating conditions. The RO plant simulation model has been used to present a proposed operational chart for the investigated desalination plant in case of working under different feed water salinity and temperature.

KEY WORDS

Hydraulic System, Axial piston pump, RO Desalination, RO membrane, Experimental Investigation, Pressure Measurement, Flowrate Measurement, Validation.

* Egyptian Armed Forces.

EXPERIMENTAL TEST RIGS

The experimental work has been carried out on a real RO desalination plant commonly used in Egypt. Flowrate and pressure measurements have been done to determine the high pressure pump characteristics and the RO membrane performance under different operating parameters. The experimental measurements have been used to evaluate the validity of the proposed simulation model programmed in part 1 of this paper. The experimental facilities enable to both static and dynamic measurements of hydraulic components of the real RO plant shown in Fig. 1-a.

A separate test rig has been built up for each hydraulic component of the plant considering the measuring devices to be in the suitable places to measure the static characteristics of all desalination plant components, under various operating conditions. The test rig consists of two main groups:

- The operating hydraulic system incorporating the component under test,
- The measuring devices for data acquisition.

The system of a separate test rig consists of the following elements; a storage tank; a booster pump; a throttle valve beside the selected component under test. The details of test arrangement for individual components are presented in Ref. (Seoudy, 2003).

The instruments used for measurements of the characteristics of individual hydraulic component are shown in Fig. 1-b which includes the following instruments: Flow Meter transmitter, Pressure Transmitter, High pressure transmitter, Conductivity transmitter, and Tachometer.

Calibration steps for all measuring devices and their calibration results are presented in Ref. (Seoudy, 2003), in App. I. The data acquisition system, shown in Fig. 2-a, consists of a data acquisition card, a microprocessor, and an industrial computer. The data acquisition card is an analog to digital A/D input card. It contains eight analog input channels with 8-bit line for each channel. This card is installed in a control panel containing another input and output cards. All cards are connected and controlled by a microprocessor. The microprocessor is connected to an industrial computer. The transducers are connected directly to the (A/D) input card. Specifications of data acquisition system are presented in Fig. 2-b.

The circuit diagram of the real RO desalination plant and the individual flowrate and pressure measurement places are shown in Fig. 3. The specifications of the data acquisition system for dynamic measurements are presented in a separate sheet at the end of this paper. Error analysis has been done to all measured data and is presented in Ref. (Seoudy, 2003), in App. I.

STATIC CHARACTERISTICS MEASUREMENT

Booster Pump Test Rig

The arrangement of measuring instruments is presented in Fig. 4, The flow starts from the storage tank which contains a sufficient amount of water, the booster pump transfers the water from the tank in the piping system, then the water flows back to the

tank passing through a flow control valve which adjusts the discharged flowrate from the booster pump. The pressure and flow meter transducers are attached at the suction and delivery lines of the pump to measure the pump parameters. The tachometer is attached to the pump shaft to measure the pump speed at each tested flowrate (0 to 15 m³/hr). The effect of speed variation is considered to correct the measured head and flowrate for the pump.

Figure 5. shows a comparison between the booster pump characteristics introduced by manufacturer, measuring results, and proposes empirical formula results from experimental work. The measurements have been done up to the minimum pumping load due to the hydraulic circuit piping. This figure shows a good agreement between manufacturer, measuring results, and proposed empirical formula at range of operation.

Filtration Group Test Rig

Figure 6 presents the test rig hydraulic cycle for multi-media, activated carbon, and cartage filter. The used devices for measuring the filters characteristics are a flow meter transducer, and two pressure transducers. The arrangement of measuring instruments could be shown in Ref. (Seoudy, 2003), chapter 3. The input and output pressures are measured at different flowrates (5 to 15 m³/hr). The pressure drop versus flowrate characteristics of the filtration unit components have been plotted and curve fitted to determine the filtration unit components coefficients. Figures 7, 8, and 9 show the experimental results and curve fitting for each filter. The figures show that the pressure drop (by curve fitting) is a polynomial especially at high flow rate due to filter body but at the working range the pressure drop becomes linear.

- Curve fitting for Multi-media filter gives: $\Delta p_{mmf} = 0.005382 \times Q^2 - 0.009967 \times Q$
- Curve fitting for activated carbon filter gives: $\Delta p_{cf} = 0.003214 \times Q^2 - 0.01103 \times Q$
- Curve fitting for cartridge filter gives :
 $\Delta p_{carf} = 0.002154 \times Q^2 - 0.0005722 \times Q$

where, Δp in (bar), and Q in (m³/hr).

Characteristics of the High Pressure Pump:

Fig. 10 presents the hydraulic test rig used for measuring the characteristics of the high pressure pump. The suction pressure, the delivery pressure, the suction flowrate and the delivery flowrate at various pump pressures (0 to 70 bar) have been measured to plot the pump delivery pressure-flowrate curve. The pressure-flowrate characteristic of the high pressure pump is used to determine the pump leakage at different operating pressures. Experimental tests have shown that the volumetric losses at operating pressure of 70 bar is equal to 4.65%. The pump characteristic equation obtained by curve fitting of the experimental measurements has the following form:

$$Q_{HPP} = 10.384 - 0.0069 p \quad (m^3 / hr, bar)$$

Figure 11 shows the experimental results of the high pressure pump and the corresponding curve fitting operation. These results are used in the determination of pump dynamic model

Characteristics of Reverse Osmosis Membrane

The measuring devices for obtaining the membrane characteristics are, two flow meter transducers, two high pressure transducers, and conductivity transducer. Arrangement of the measuring instruments is as shown in Fig. 12. The water flows in closed circuit starting from the storage tank, which contains a sufficient amount of artificial seawater (Na Cl equivalent) and goes throughout the booster pump, the filtration group, and the high pressure pump, then to the membrane inlet section. Both concentrate and permeate water lines are directed to the storage tank again. The high pressure transducers are attached to the feed (inlet) and concentrated sides of the membrane. The flow meter transducer and conductivity transducer are attached to the permeate side of the membrane. Another flow meter transducer is attached to the suction line of the piston pump (booster pump exit) to measure the feed water flowrate.

The tested Membrane and measuring devices are shown in Fig. 13 and Fig. 14. The measurements have been carried out to measure the total dissolved solids, and the temperature in artificial seawater. The feed pressure has been adjusted at certain value by using the throttle valve. The concentrate pressure, the feed flowrate, the permeate flowrate, and the permeate conductivity have been measured at feed pressures ranges from 30 to 60 bar. The measurements have been repeated three times with three different artificial seawater concentrations (21000 ppm, 28900 ppm, and 33000 ppm NaCl). The used NaCl specifications are presented in Ref (Seoudy, 2003), in App. L

DYNAMIC CHARACTERISTICS MEASUREMENT

Test rig and Instrumentation

The same test rig used in static characteristic measurement has been used also to measure the dynamic characteristics of the high-pressure piston pump. The data acquisition system in this case is of higher sampling rate to be able to measure the high piston pressure fluctuations at several operating pressures under different conditions. The measuring sensor is a calibrated high-pressure transducer. The data acquisition system consists of a data acquisition card, a terminal board, and a personal computer. The data acquisition card is an analog to digital (A/D) and digital to analog (D/A) card. It contains one digital to analog channel with unipolar or bipolar format, and eight analog to digital channels with unipolar or bipolar format with 12-bit line for each channel. The card is installed in a personal computer and is connected to the terminal board by the data cable. The A/D – D/A terminal board provides terminals for connecting analog or digital I/O signals. It consists of two digital to analog terminals and 16 analog to digital terminals, which provide single-ended analog to digital connectors. The terminal board is connected to the A/D – D/A card by a 25 pin flat cable. The specification of the data acquisition system is presented in Ref. (Seoudy, 2003), in App. M. The A/D – D/A card is installed in the PC motherboard. The PC controls the A/D-D/A card to receive the data through the software program “SIMULINK”. Also, it is used in collecting and saving data. The SIMULINK model is shown in Fig. 15. The analog output signal of the pressure transducer has current

intensity of 0÷20 mA. The data acquisition card receives an analog signal voltage of -5 ÷ 5 V. Signal current has been converted to volt in order to receive the data by the data acquisition card. A simple resistance (250 Ω) is used to convert the signal current to volt as shown in Fig. 16 and Fig. 17.

High Pressure Pumping Unit

The measurement are carried out by measuring of pressure fluctuations in the delivery line of the pump with and without accumulator in the hydraulic circuit at pump pressure ranges (30 to 60 bar). The measured data have been used to plot the fluctuations in pump pressure. The experimental results are plotted in Fig. 17 and Fig. 18. Fig. 17 presents the experimental results of the piston pump with connecting an empty accumulator to the circuit. Fig. 18 presents the experimental results of the piston pump with eliminating the accumulator from the circuit.

The experimental measurements show that, the accumulator has a good effect in decreases pressure fluctuations in the hydraulic circuit, even when it is empty.

PERFORMANCE PREDICTION AT OFF DESIGN CONDITIONS

Simulation model of the high-pressure pump could be used to investigate the dynamic behavior in case of working with presence of failure in one of pump components. Expected failures are such as sticking of one delivery valve or excessive leakage in a cylinder of pump pistons. Membrane simulation model could be used to investigate the membrane performance with the change in operating conditions, such as feed water salinity or feed water temperature. The membrane simulation model has been used to present a proposed operating chart for the desalination plant at different water salinity and temperature.

High Pressure Pump Simulation

The high pressure pump dynamic performance is characterized by the value of flowrate irregularity coefficient, ε_Q , or pressure irregularity coefficient, ε_P , where:

$$\varepsilon_Q = \frac{Q_{\max} - Q_{\min}}{Q_{av}} \times 100\%$$

where ε_Q : Flowrate irregularity coefficient, (%); Q_{\max} : Pump maximum flowrate, (m^3/s); Q_{\min} : Pump minimum flowrate, (m^3/s); Q_{av} : Pump average flowrate, (m^3/s).

To predict the off design conditions, the following cases have been simulated:

- A. Piston pump with charged accumulator, as shown in Fig. 19 and Fig. 20.
- B. Piston pump with charged accumulator while one delivery valve is sticking, as shown in Fig. 21 and Fig. 22.
- C. Piston pump with an empty accumulator while one delivery valve is sticking, as shown in Fig. 23 and Fig. 24.
- D. Piston pump with charged accumulator while excessive leakage at one chamber occurs, as shown in Fig. 25 and Fig. 26.

- E. Piston pump with an empty accumulator at while excessive leakage at one chamber occurs, , as shown in Fig. 27 and Fig. 28.
- F. Piston pump without accumulator while one delivery valve is sticking, , as shown in Fig. 29 and Fig. 30.
- G. Piston pump without accumulator while excessive leakage at one chamber occurs, as shown in Fig. 31 and Fig. 32.

Results and Discussion

The dynamic model simulates to a great extent the high pressure pump flowrate and pressure fluctuations at different conditions. The results showed that the pump performance may be characterized by both the irregularity coefficients of flowrate, ϵ_Q , and pressure, ϵ_P . The flowrate and pressure irregularity coefficients are affected by any failure in the pump components. Table 1 shows the values of flowrate irregularity coefficients at different failure conditions. Table 2 shows the values of pressure irregularity coefficients at the same failure conditions.

Table 1 The values of flowrate irregularity coefficients at different failure conditions

Failure	Flowrate irregularity coefficient, ϵ_Q , (%)		
	Pump with accumulator		Pump without accumulator
	charged	empty	
No failure	15.45	14.7	13.6
One delivery valve is sticking	34.52	34.56	26.3
Excessive leakage at one chamber occurs	21.4	19.9	48.6

Table 2 The values of pressure irregularity coefficients at different failure conditions

Failure	Pressure irregularity coefficient, ϵ_P , (%)		
	Pump with accumulator		Pump without accumulator
	charged	empty	
No failure	0.1	5.83	15.3
One delivery valve sticking	1.845	21.99	47.1
Excessive leakage at one chamber occurs	0.7	11.9	20.2

The measured pressure irregularity has a value of 5.5% (with empty accumulator) and 15% (without accumulator). The simulation results of the pressure irregularity show good agreement with the measured values, so this simulation model could be considered for more theoretical investigations.

Membrane simulation

Mathematical equations, describing the membrane could be solved by simulation

program. The Model has been carried out using SIMULINK 4 in MATLAB 6.1. Two models are designed to study the membrane characteristics as follow:

- The first model is designed to study the effect of feed pressure on the membrane performance parameters.
- The second model is designed to study the effect of system recovery ratio on the membrane performance parameters.

Figures from 33 to 38 present some of the simulated model variables. There are factors having a various effects on the operational conditions of the membrane performance. Simulation programs present the effect of, the following on the membrane performance parameters:

1. Feed water salinity, feed water temperature, and recovery ratio on the membrane feed pressure.
2. Feed water salinity, feed water temperature, and feed pressure on the membrane pressure drop along the membrane length, and the permeate flowrate.

The effects of operational conditions on the membrane performance parameters could be studied by using the simulation programs as follows:

- **Effect of changing feed water salinity.** Figure 33 represents the effect of changing feed water salinity on the feed pressure delivered to the membrane. To study the effect of changing feed water salinity on the feed pressure, at various feed water flowrates, the following assumptions are considered:

1. Constant feed water temperature.
2. Constant recovery ratio

Simulation results show that at certain feed flowrate, the feed pressure is directly proportional to the feed water salinity. The change of feed water salinity alters two main parameters which affect the feed pressure:

1. Feed water osmotic pressure (π_f).
2. Average membrane permeability ($\bar{A}(\bar{\pi})$).

As feed water salinity increases the feed water osmotic pressure (π_f) increases because of the increase of ion concentration of feed water. While the average membrane permeability ($\bar{A}(\bar{\pi})$) decreases because when the feed water salinity increases, the feed water density increases as the dissolved ions in the same feed water quantity increase. Therefore the viscosity of the feed water increases. So the average membrane permeability decreases, i.e., more pressure is needed to overcome the decrease in permeability to allow the same amount of permeate flow to pass though the membrane. Fig. 34, shows the effect of changing of feed water salinity on average membrane permeability and feed osmotic pressure.

- **Effect of changing feed water temperature.** Figure 35 represents the effect of changing feed water temperature on the feed pressure of the membrane. To study of the effect of changing feed water temperature on feed pressure, at various feed water flowrates, the following assumptions are considered:

1. Constant feed water salinity.
2. Constant recovery ratio.

Simulation results show that at certain feed flowrate the feed pressure is inversely proportional to the feed water temperature. The feed pressure decreases as feed water temperature increases due to:

1. Increase of the temperature correction factor (TCF).
2. Increase of feed water osmotic pressure (π_f) as the feed water temperature increases.
3. Decrease of average membrane permeability ($\bar{A}(\bar{\pi})$).

The increase in feed water osmotic pressure doesn't cause an increase in feed pressure as expected. The decrease in feed pressure is mainly due to the increase of the temperature correction factor. The decrease of average membrane permeability has a slight effect on the decrease of feed pressure as shown in Fig. 36.

▪ **Effect of changing recovery ratio.** Fig. 37 represents the effect of changing recovery ratio (permeate flowrate / feed flowrate) on the feed pressure of the membrane. To study of the effect of changing of recovery ratio on feed pressure at different feed water flowrates, the following assumptions are considered:

1. Constant feed water salinity.
2. Constant feed water temperature.

Simulation results show that at certain feed flowrate the feed pressure is directly proportional to the recovery ratio.

The operating pressure increases as recovery ratio increases due to:

1. Decrease of average concentrate-side system pressure drop (ΔP_{fc}) due to the decrease of average feed-concentrate flowrate (q_{fc}).
2. Decrease of average membrane permeability $\bar{A}(\bar{\pi})$, as q_{fc} decreases the membrane boundary layer has more ions concentration, i.e. the average concentrations polarization factor (pf) increases, so the average concentrate-side concentration (C_{fc}) increases and causes the decrease in ($\bar{A}(\bar{\pi})$).

Membrane Performance

The two parameters that characterize the membrane performance from both quality and quantity point of view are:

- **Permeate Flux:** the rate of permeate transported per unit area of membrane, usually measured in liter per square meter per hour ($l/m^2.h$).
- **Salt Rejection:** the percentage of solids concentration removed by the membrane from the feed water.

The main parameters affecting membrane performance are:

- Feed water salinity
- System recovery ratio
- Feed water pressure
- Feed water temperature

Figures from 39 to 42 show the effect of these parameters on permeates flux and salt rejection.

- **Effect of feed water salinity on RO membrane performance.** Figure 39 represents the effect of the feed water salinity on the permeate flux and salt rejection. The simulation result shows that both permeate flux and salt rejection

decreases with the increase of feed water salinity. The rate of decrease of permeate flux with the increase of feed water salinity is almost linear. The rate of decrease of salt rejection with the increase of feed water salinity is nonlinear. The salt rejection decreases due to the increase of membrane permeability. The permeate flux decreases also, although the permeability increases, because of the increase of osmotic pressure which decreases the net driving pressure.

- **Effect of system recovery ratio on RO membrane performance.** Figure 40 represents the effect of the system recovery ratio on the permeate flux and salt rejection. The simulation results show that both permeate flux and salt rejection increases with the increase of system recovery ratio. The rate of increase of permeate flux with the increase of system recovery ratio is almost linear. The rate of increase of salt rejection with the increase of system recovery ratio is nonlinear. The change of the salt rejection is due to the increase of the concentration polarization at the membrane surface. So it increases the osmotic pressure and increases the feed pressure consequently, the permeate flux increases linearly with the increase of system recovery ratio and then affects the salt rejection to increase.
- **Effect of feed water pressure on RO membrane performance.** Figure 41 represents the effect of the feed water pressure on the permeate flux and salt rejection. The simulation results show that both permeate flux and salt rejection increases with the increase of feed water pressure. The rate of increase of permeate flux with the increase of feed water pressure is almost linear. The rate of increase of salt rejection is sharp for feed pressures up to 50 bar then the rate of increase is so slow and reach to an approximately constant value at feed pressure of 70 bar. The behavior of salt rejection increase is due to the increase of net driving pressure which increases the permeate flux. The salt rejection reaches a constant value at high feed pressure because RO membranes are imperfect barriers to the dissolved salts in feed water; there are always some salt passages through the membrane. As the feed pressure is increased, these salt passages are increasingly overcome as water is pushed through the membrane at a faster rate than salt can be transported. However, there is an upper limit to the amount of salt that can be excluded via increasing of feed pressure. As the salt rejection curve in Fig. 41 indicates; above a certain pressure level, salt rejection no longer increases and some salt flow remains coupled with water flow through the membrane.
- **Effect of feed water temperature on RO membrane performance.** Figure 42 represents the effect of the feed water temperature on the permeate flux and salt rejection. Simulation results show that the permeate flux increases with the increase of feed water temperature and salt rejection decreases with the increase of feed water temperature. The rates of increase of permeate flux and the rates of decrease of salt rejection with the increase of feed water pressure are nonlinear. The decrease of salt rejection is due to the increase of membrane permeability coefficient, so more ions of salt can pass through the membrane.

Results and Discussion

One of the main benefits of the simulation model of the reverse osmosis is to determine the recommended operating feed pressure range for the reverse osmosis plant. Operation pressure is determined according to the following:

- The maximum feed pressure depends on the maximum manufacturer recommended feed pressure for the membrane physical characteristics.
- The minimum feed pressure depends on the maximum average osmotic pressure, to avoid reverse flow in the membrane.

Fig. 43 shows the simulation results of determining the maximum and minimum feed pressures for the selected RO plant using the simulation program at feed water salinity of 35000 ppm and water temperature of 22 °C. Table 3 show the maximum, minimum operating pressure and the corresponding recovery ratio and permeate flux values results from the simulation program. Figures 44, 45, and 46 show the suggested operating charts (feed pressure and % of salt rejection vs. recovery ratio) for different salinities and different water temperatures.

Table 3, Max. and Min. Values of operating parameters

	Pressure (bar)	Recovery ratio (%)	Permeate flux (L/m ² /hr)
Max.	65	31	17.14
Min.	45	17	7.27

CONCLUSIONS

The following findings are concluded from the present investigation:

- 1- The presence of an accumulator in the system is strongly affecting the piston pump pressure irregularity coefficient, ϵ_p .
- 2- The presence of charged accumulator in the system may be useful in decreases the bad effect of abnormal operation of the piston pump.
- 3- The RO membrane permeability could be consider as the main factor that affects the operating pressure of the RO membrane when changing in feed water salinity, feed water temperature, or recovery ratio occur.
- 4- The following parameters should be considered when determining the operating pressure for the RO plant:
 - The physical characteristics of the membrane material,
 - The osmotic pressure at the membrane concentration exit.
- 5- The theoretical investigation of the membrane showed that, the effect of water temperature on the operating pressure could be neglected, while the recovery ratio is increased from 17% to 31% when temperature increases from 18°C to 26°C. When the temperature is increased from 18°C to 26°C the following parameters are predicted:
 - Operating pressure decreases from 63 bar to 56 bar for water salinity 30000ppm at 3.74 m³/hr permeate water.
 - Operating pressure decreases from 63 bar to 57 bar for water salinity 35000ppm at 3.08 m³/hr permeate water.
 - Operating pressure decreases from 63 bar to 57.5 bar for water salinity 40000ppm at 2.53 m³/hr permeate water.

REFERENCES

1. Al-Bastaki, N. M., and Abbas, A., "Predicting The Performance Of Ro Membranes", Conference On Membranes In Drinking and Industrial Water Production, L'Aquila, Italy, Vol. 2, pp 397–403, October 2000.
2. Al-Shayji, Khawla Abdulmohsen, "Modeling, Simulation, And Optimization of Large-Scale Commercial Desalination Plants", Ph.D thesis, Virginia Polytechnic Institute and State University, USA, 1998.
3. Cherkassky, V.M., "Pumps, Fans and Compressors", Mir Publishers, Moscow, 1985.
4. Dow Chemical Company "FILMTEC Membrane" Technical Manual, April 1995.
5. Etsion, I., and Magen, M. "Piston Vibration in Piston-Cylinder Systems", Transaction of the ASME Journal of Fluid Engineering, Vol, 87, pp 214-221, March.1980.
6. Goulds Pump Company "Technical Manual", USA, 1998.
7. Hanbury, W.T., Hodgkiess, T., and Morris, R., "Desalination Technology", Intensive Course Manual, Porthan Ltd.- Easter Auchinloch, Glasgow, UK 1993.
8. Harris, R. M., Edge, K. A., And Tilley, D. G., "The Suction Dynamics Of Positive Displacement Axial Piston Pumps" Transaction of the ASME Journal of Dynamic System, Measurement and Control, Vol. 116, No. 1, pp 281-287, 1994.
9. Karassik, I. J., Messina, J. P., Cooper, P., Heald, C. C., "PUMP HAND BOOK", Third Edition , JON WILEY & SONS, INC., 1999.
10. Nakano, H. , Machiyama, T., and Kawase, T. "Modelling Of The Generation Mechanism Of Flow Pulsation's By An Axial Piston Pump" Bulletin of the JSME, Vol. 26, No. 175, pp. 203-208, 1986.
11. Seoudy, A., "Simulation of R.O. Seawater Desalination System", M.Sc. thesis, Military Technical College, Cairo, Egypt, 2003.
12. Stepanoff, A.J., "Centrifugal And Axial Flow Pumps", John Wiley, New York, 1967.
13. Taniguchi, M., Kurihara, M., and Kimura, S., "Behavior Of A Reverse Osmosis Plant Adopting A Brine Conversion Two-Stage Process And Its Computer Simulation", Journal of Membrane Science, Vol. 183, pp 249–257, 2001.
14. Wheatly Gaso Inc. "Wheatley Pumps" Operator's Manual, USA, 1996.

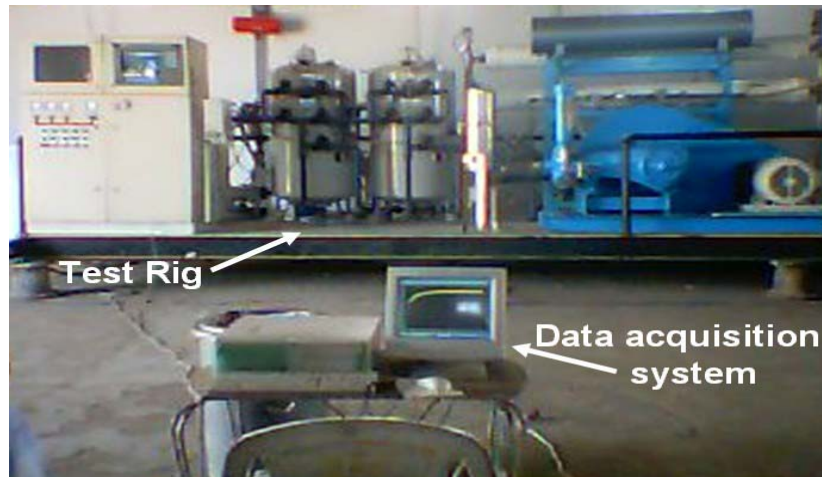


Fig. 1 Photo of the hydraulic system of real RO plant (test rig) connected to the data acquisition system.

1. Flow Meter transmitter:

- Type : In line Digital Flow Transmitter
- Manufacture : burkert.
- Model : 8035 Plastic-INLINE
- Pipe diameter : 1.5 "
- Measuring range : 0 – 25 , 0 – 10 m³/hr.
- Measuring error : ±0.5%
- Voltage supply : 12...30 VDC.
- Output signal : 4...20 mA



2. Pressure Transmitter:

- Type : piezoresistive Transmitter
- Manufacture : burkert.
- Model : 8320
- Material : stainless steel 316
- Measuring range : 0 – 10 bar.
- Accuracy % : < 1%
- Voltage supply : 12...30 VDC.
- Output signal : 4...20 mA



3. High pressure transmitter

- Type : Thin film
- Manufacture : Tectis
- Model : 3377
- Material : stainless steel 316
- Measuring range : 0 – 100bar.
- Accuracy % : ±0.25%
- Response time : ≤ 1 ms
- Voltage supply : 12...30 VDC.
- Output signal : 4...20 mA



4. Conductivity transmitter:

- Manufacture : burkert.
- Model : 8225
- Material : PVC
- Electrode material : stainless steel electrode
- Measuring range : 0 – 5000 ppm.
- Measuring error : typical: 3 % of measured value
max.: 5 % of measured value
- Voltage supply : 12...30 VDC.
- Output signal : 4...20 mA



5. Tachometer:

- Type : Digital photo tachometer.
- Test range : 5 to 100,000 rpm.
- Resolution : 1 rpm.
- Accuracy : ± 1 rpm & + 0.05% (over 5000 rpm).
- Sampling time : 1 sec (over 60 rpm).
- Operating temperature : 0 °C to 50 °C.
- Detecting distance : 50 to 150 mm.



Fig. 1-b. Measuring Instruments used in Test rig



Fig. 2 Data acquisition system

1. Data acquisition card:

I/O connection modules can be installed in online state by pushing them to DIN rail. Modules have also plug in connectors and well readable connector numbering. Modules communicate with CPU with fast parallel bus.

Card specifications:

- 8 analog inputs
- 13bit A/D conversion
- Several sensors types eg. NTC. PT 100, NI 1000, AD590
- Transducers types 0...10VDC, 4...20 mA.



2. Microprocessor:

Type : ATMOS 88
 Manufacture : Atmostech Oy.

Microprocessor specifications:

- High performance processor with wide memory.
- With LCD-display (40x16 character) and keyboard
- Have four serial ports which can be used to communicate with burglar alarm, fire alarm or energy measurement systems.



3. Industrial computer:



Fig. 2-b. Specifications of data acquisition system

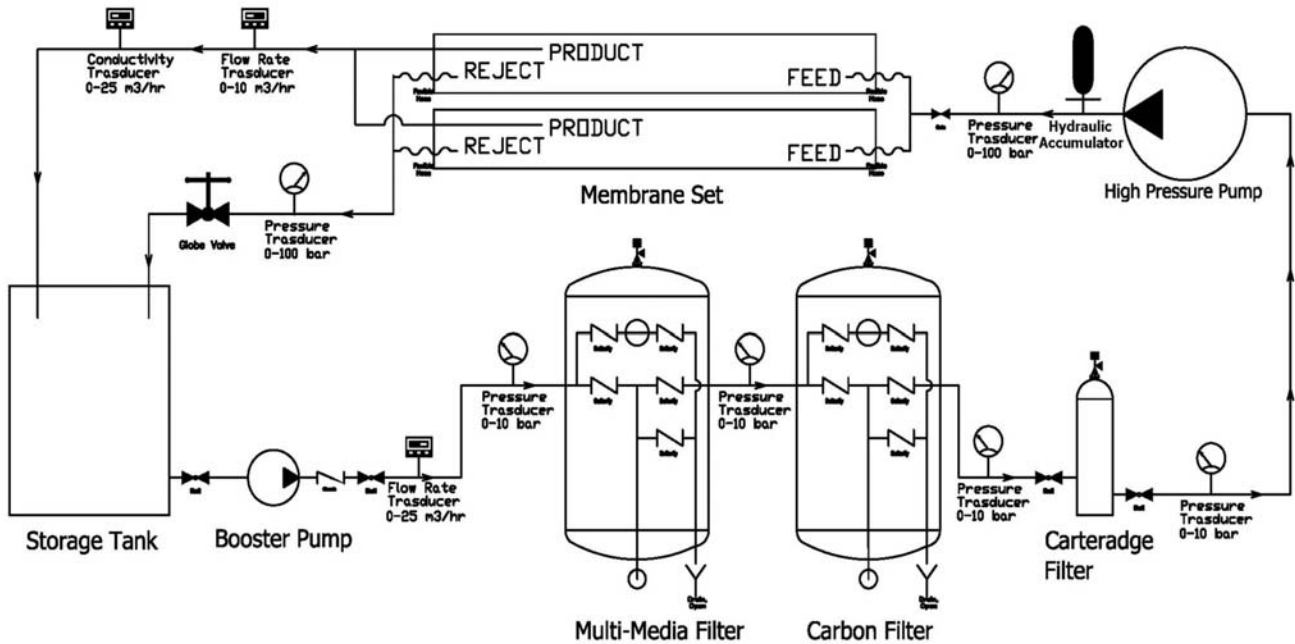


Fig. 3. Hydraulic circuit of RO plant (test rig)

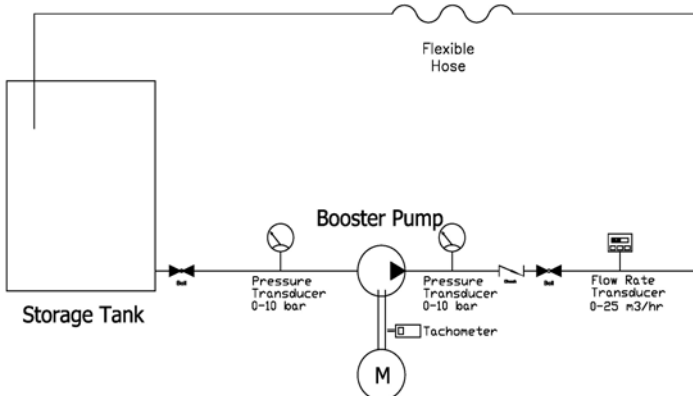


Fig. 4 Test rig of hydraulic circuit including the booster pump

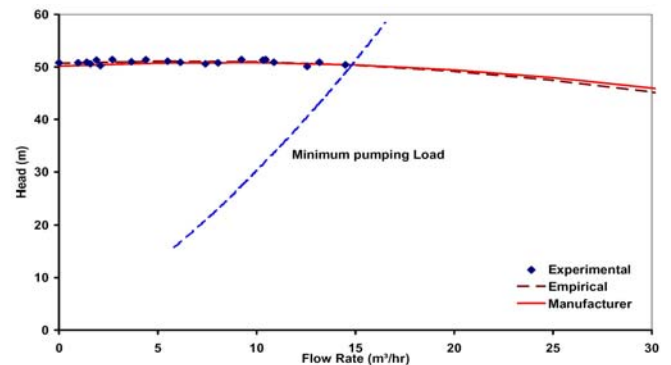


Fig. 5 Comparison between booster pump characteristics introduced by the manufacturer, the measured results, and proposes the empirical formula

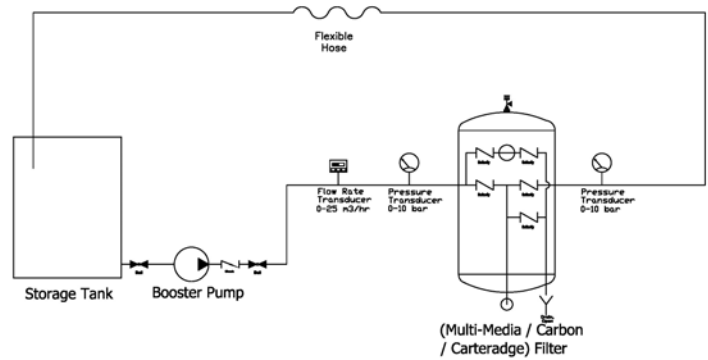


Fig. 6 Test rig of hydraulic circuit including the multi-media, the activated carbon, and the cartage filter

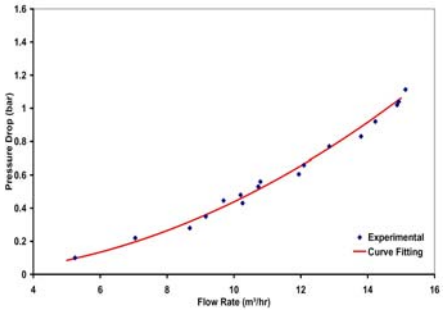


Fig. 7 Multi-media filter

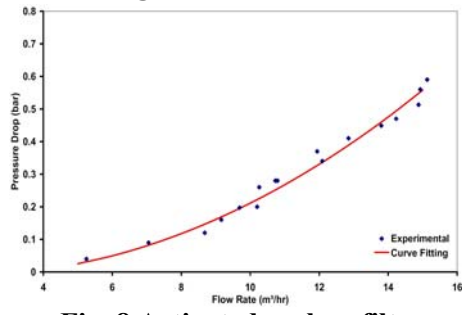


Fig. 8 Activated carbon filter

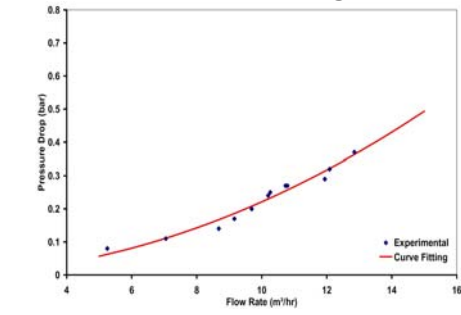


Fig. 9 Cartridge filter

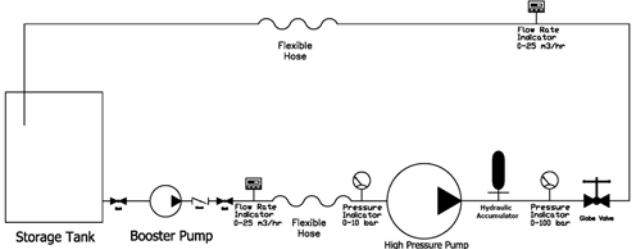


Fig. 10 Test rig of measuring the high pressure pump characteristics

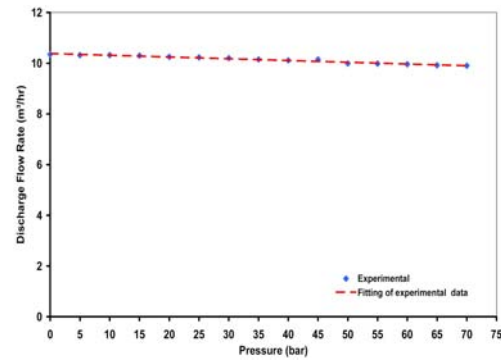


Fig. 11 high pressure pump characteristics

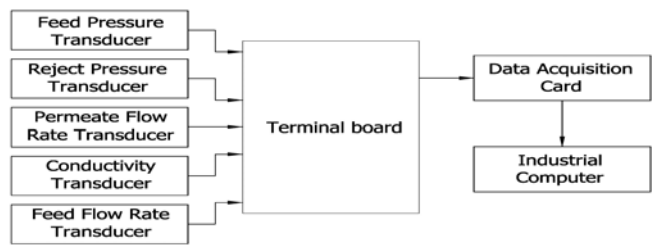


Fig. 12 Measuring instruments for testing the membrane



Fig. 13 Experimental test rig of the Membrane

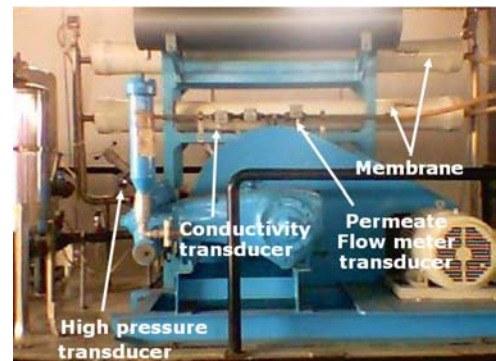


Fig. 14 The tested Membrane and measuring devices

Piston pump dynamic characteristics measuring model

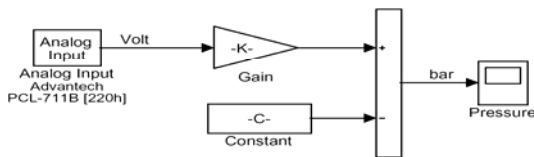


Fig. 15 SIMULINK model for the measured pressure

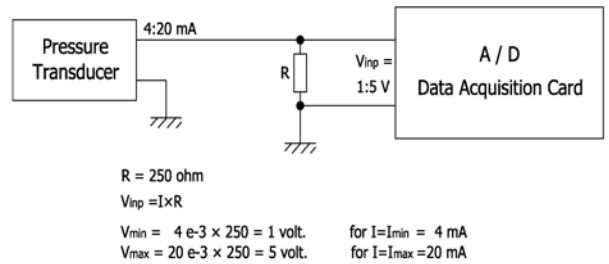


Fig. 16 Conversion of pressure signal current to volt

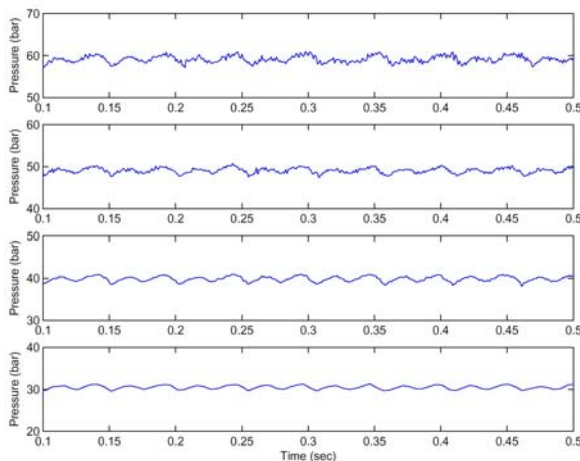


Fig.17 Experimental results of the pressure fluctuation of the piston pump with an empty accumulator at pump working pressures of 60.3, 50.8, 40, and 29.8 bar

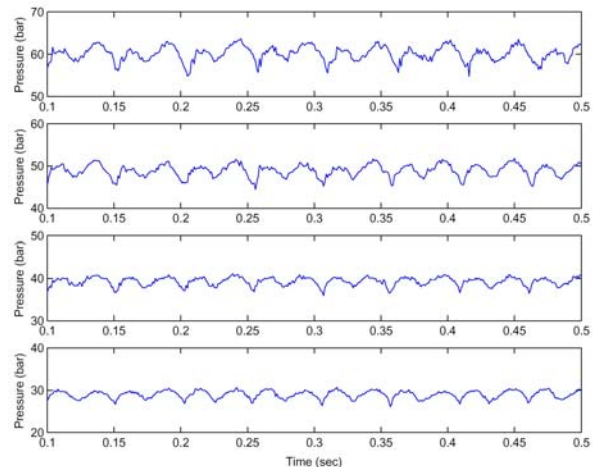


Fig. 18 Experimental results of the pressure fluctuation of the piston pump without accumulator at pump working pressures of 60.3, 50.8, 40, and 29.8 bar

A. Piston pump with charged accumulator

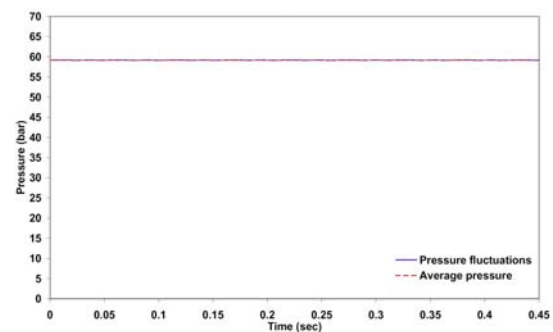
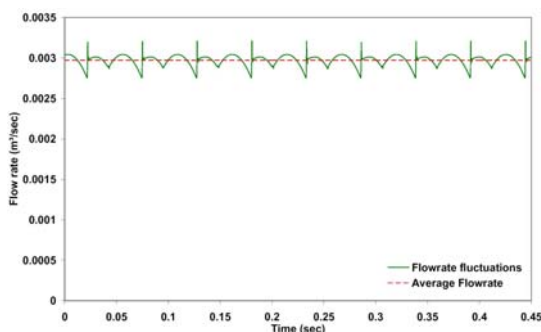


Fig. 20 Simulation of piston pump pressure

Fig. 19 Simulation of piston pump flowrate fluctuations with an accumulator charged at 30 bar, (n=227.4 rpm)

fluctuations with an accumulator charged at 30 bar, (n=227.4 rpm)

B. Piston pump with charged accumulator while one delivery valve is sticking

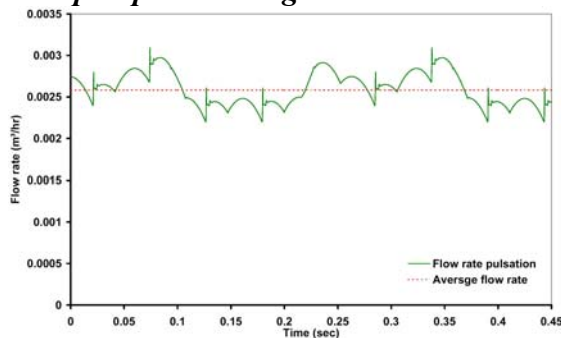


Fig. 21 Simulation of piston pump flowrate fluctuations with an accumulator charged at 30 bar while one delivery valve is sticking, (n=227.4 rpm)

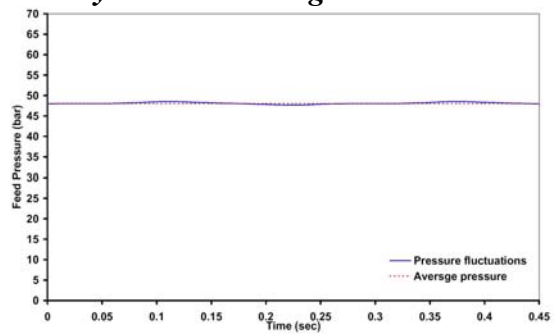


Fig. 22 Simulation of piston pump pressure fluctuations with an accumulator charged at 30 bar while one delivery valve is sticking, (n=227.4 rpm)

C. Piston pump with an empty accumulator while one delivery valve is sticking

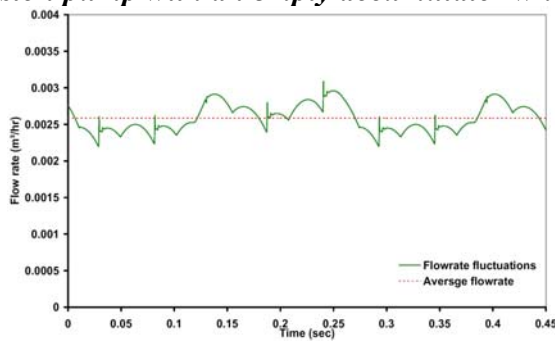


Fig. 23 Simulation of piston pump flowrate fluctuations with an empty accumulator while one delivery valve is sticking, (n=227.4 rpm)

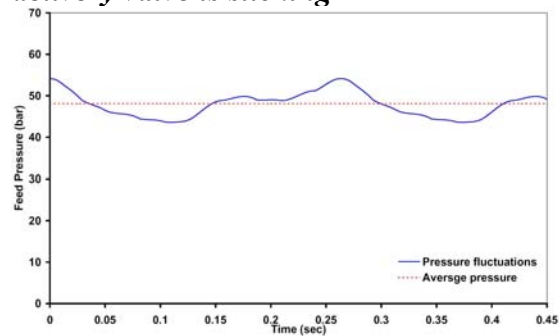


Fig. 24 Simulation of piston pump pressure fluctuations with an empty accumulator while one delivery valve is sticking, (n=227.4 rpm)

D. Piston pump with charged accumulator while excessive leakage at one chamber occurs

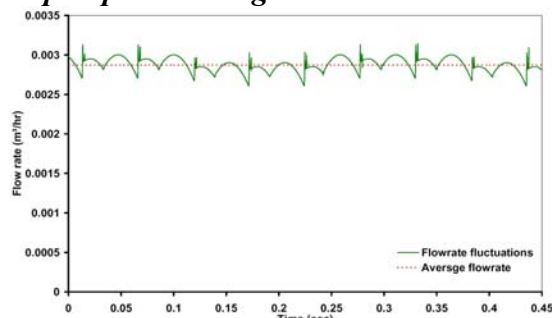


Fig. 25 Simulation of piston pump flowrate fluctuations with charged accumulator at 30 bar while excessive leakage at one chamber occurs, (n=227.4 rpm)

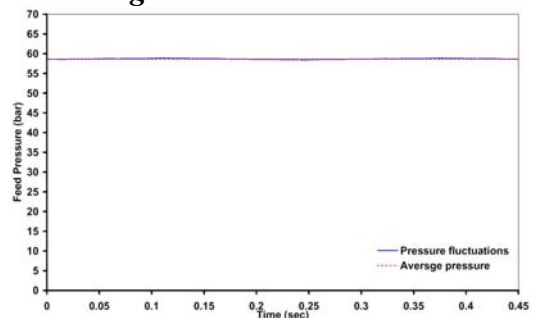


Fig. 26 Simulation of piston pump pressure fluctuations with charged accumulator at 30 bar while excessive leakage at one chamber occurs, (n=227.4 rpm)

E. Piston pump with an empty accumulator at while excessive leakage at one chamber occurs

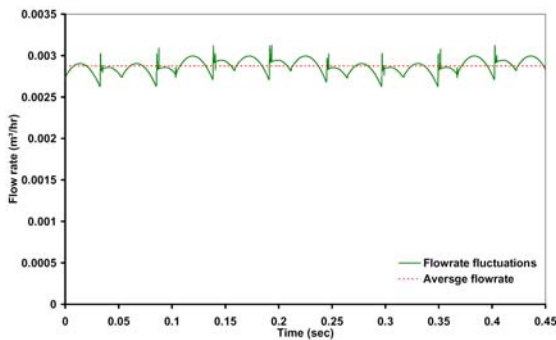


Fig. 27 Simulation of piston pump flowrate fluctuations with an empty accumulator while excessive leakage at one chamber occurs, (n=227.4 rpm)

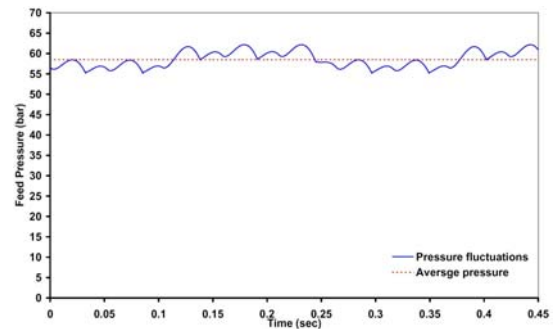


Fig. 28 Simulation of piston pump pressure fluctuations with an empty accumulator while excessive leakage at one chamber occurs, (n=227.4 rpm)

F. Piston pump without accumulator while one delivery valve is sticking

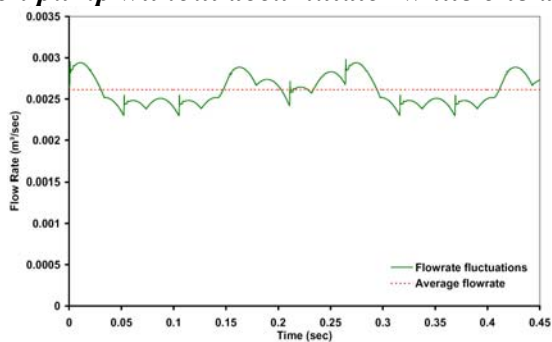


Fig. 29 Simulation of piston pump flowrate fluctuations without accumulator while one delivery valve is sticking, (n=227.4 rpm)

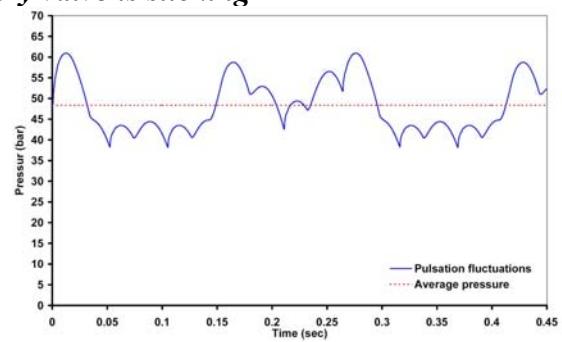


Fig. 30 Simulation of piston pump pressure fluctuations without accumulator while one delivery valve is sticking, (n=227.4 rpm)

G. Piston pump without accumulator while excessive leakage at one chamber occurs

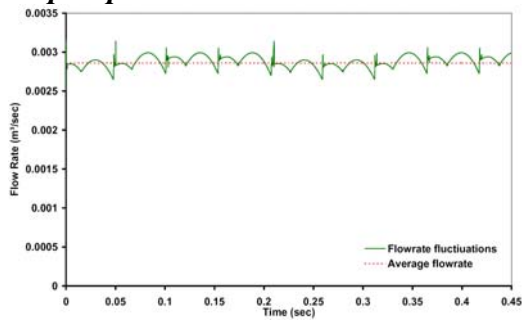


Fig. 31 Simulation of piston pump flowrate fluctuations without accumulator while excessive leakage at one chamber occurs, (n=227.4 rpm)

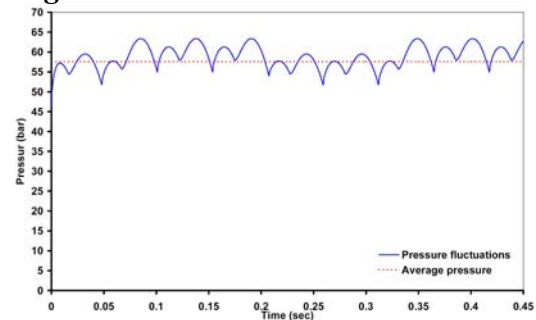


Fig. 32 Simulation of piston pump pressure fluctuations without accumulator while excessive leakage at one chamber occurs, (n=227.4 rpm)

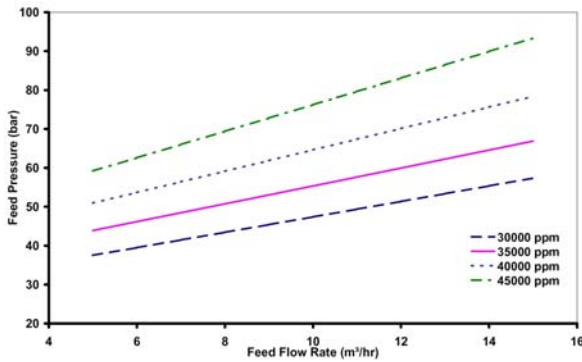


Fig. 33 Membrane characteristic curve (feed pressure vs. feed flowrate) salinity effect on feed pressure at sater temperature of 22 °C, and recovery ratio of 25%

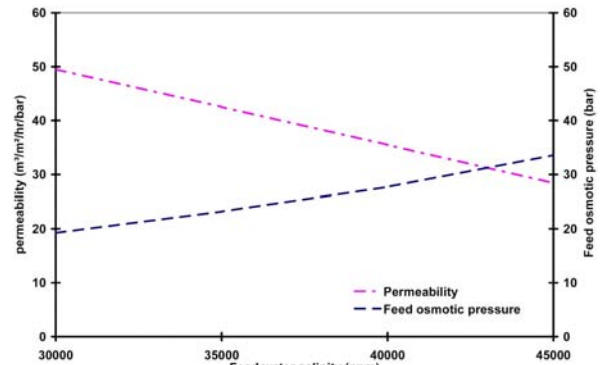


Fig. 34 Effect of feed water salinity on permeability and feed osmotic pressure at constant feed flowrate

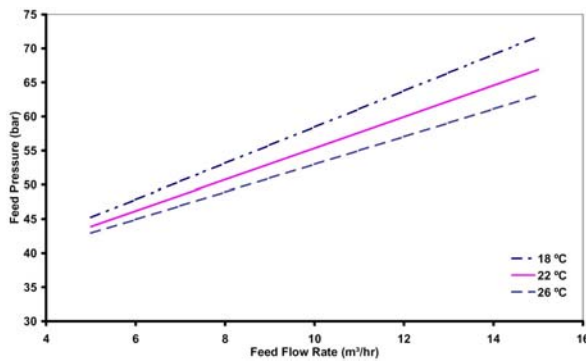


Fig. 35 Membrane characteristic curve (feed pressure vs. feed flowrate) temperature effect on operating pressure at water salinity of 35000 ppm and recovery ratio of 25%

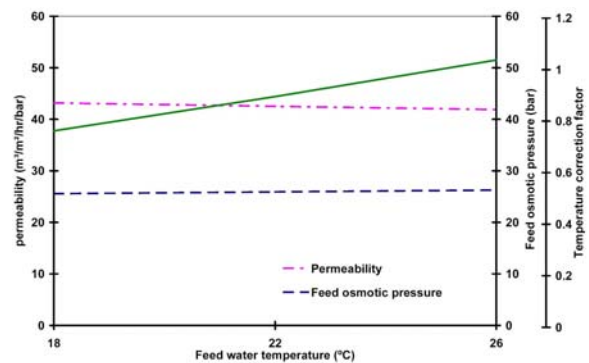


Fig. 36 Effect of feed water temperature on permeability, feed osmotic pressure, and temperature correction factor at constant feed flowrate

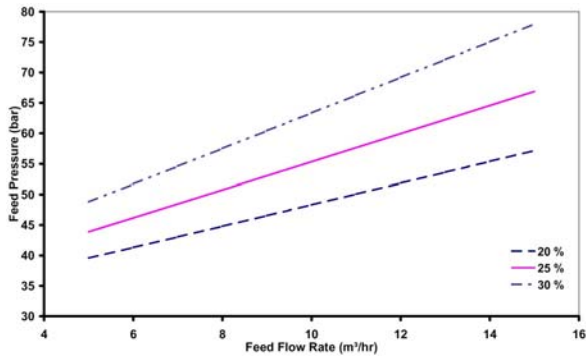


Fig. 37 Membrane characteristic curve (feed pressure vs. flowrate) recovery ratio effect on operating pressure at water salinity of 35000 ppm, and water temperature of 22 °C

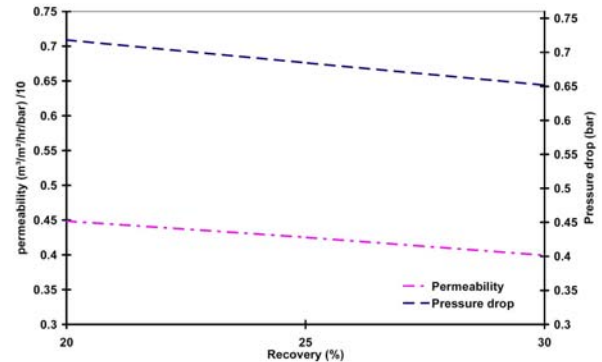


Fig. 38 Effect of recovery ratio at permeability and pressure drop at constant feed flowrate

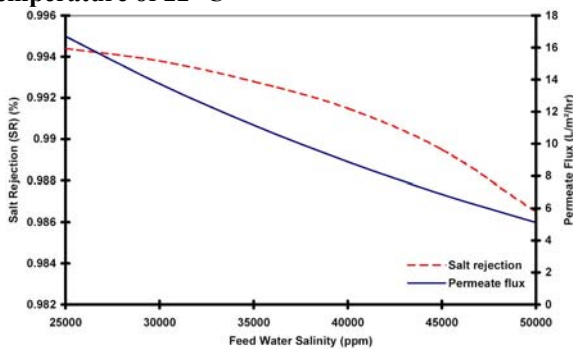


Fig. 39 Membrane characteristic curve (salt rejection & permeate flux vs. feed water salinity) at water temperature of 22 °C, feed flowrate of 10 m³/hr, and feed pressure of 58 bar

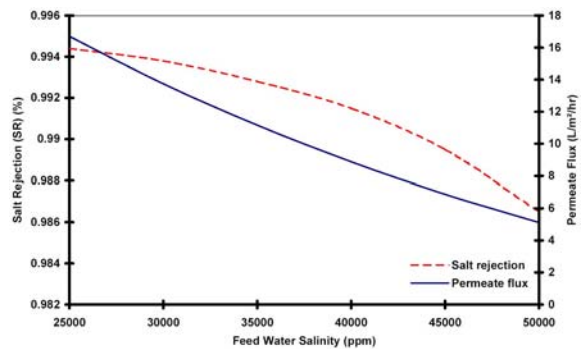


Fig. 40 Membrane characteristic curve (salt rejection & permeate flux vs. recovery ratio) at water temperature of 22 °C, feed flowrate of 10 m³/hr, and feed water salinity of 35000 ppm

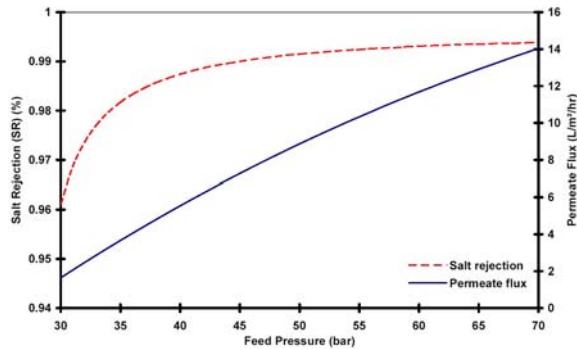


Fig. 41 Membrane characteristic curve (salt rejection & permeate flux vs. feed pressure) at water temperature of 22 °C, feed flowrate of 10 m³/hr, and feed water salinity of 35000 ppm

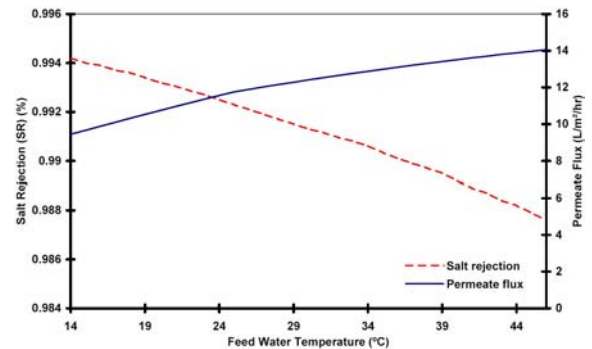


Fig. 42 Membrane characteristic curve (salt rejection & permeate flux vs. feed water temperature) at feed pressure of 58 bar, feed flowrate of 10 m³/hr, and feed water salinity of 35000 ppm

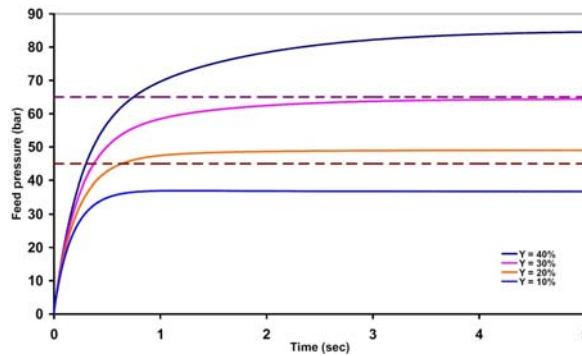


Fig. 43 Maximum and minimum allowed operation pressure at feed water salinity of 35000 ppm, and water temperature of 22 °C

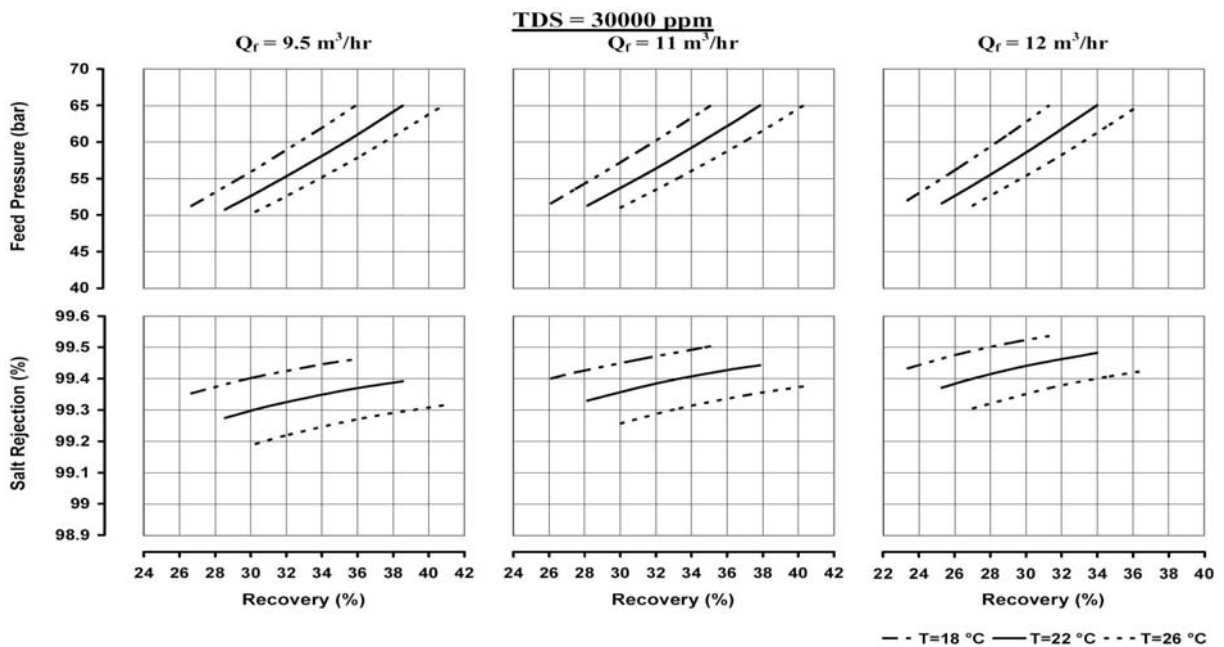


Fig. 44 Maximum and minimum feed pressure for feed water salinity 30000 ppm

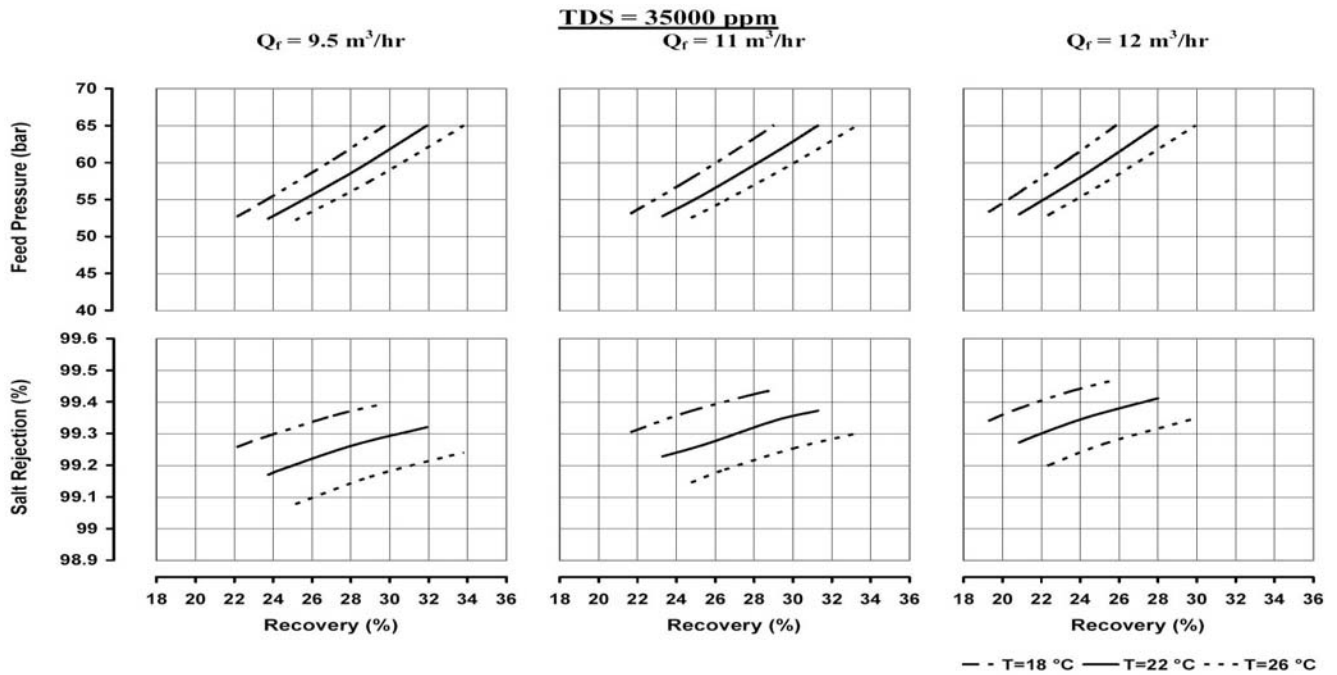


Fig. 45 Maximum and minimum feed pressure for feed water salinity 35000 ppm.

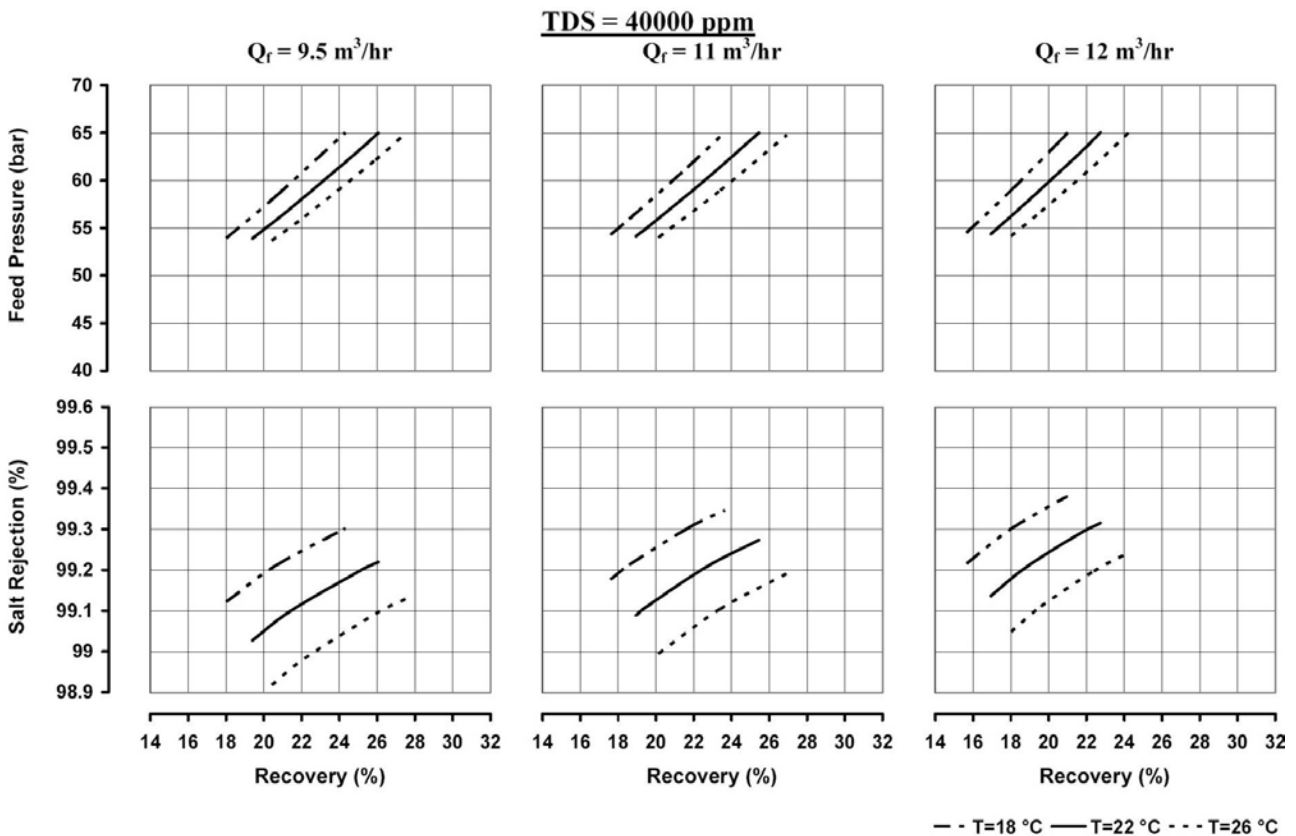


Fig. 46 Maximum and minimum feed pressure for feed water salinity 40000 ppm

Data acquisition system specifications for dynamic measurements

Features:

- 12-bit resolution A/D conversion
- Accepts 8 single-ended analog inputs
- Programmable analog input ranges: $\pm 5V$, $\pm 2.5V$, $\pm 1.25V$, $\pm 0.625V$, $\pm 0.3125V$
- Support software trigger, programmable pacer trigger, and external trigger

- Programmable IRQ level for A/D data transfer
- One 12-bit multiplying D/A output channel, with the output range of 0 to +5V or 0 to +10V
- On-board 16-bit digital output
- Versatile language drivers including BASIC, PASCAL, C and C++

Analog Input (A/D Converter):

Channels	: 8 single-ended inputs.
Resolution	: 12 bits, successive approximation.
Input range	: $\pm 5V$, $\pm 2.5V$, $\pm 1.25V$, $\pm 0.625V$ and $\pm 0.3125V$ soft ware programmable.
Converter	: AD574 or equivalent.
Conversion time	: 25 μ s max.
Accuracy	: 0.015% of reading ± 1 LSB.
Nonlinearity	: ± 1 bit.
Amplification gains	: $\times 1$, $\times 2$, $\times 4$, $\times 8$, and $\times 16$, soft ware programmable.
Trigger mode	: By soft ware, pacer and external trigger.
Data transfer	: By soft ware or interrupt.
Over voltage	: Continuous $\pm 30V$ max.
IRQ level	: IRQ2 to IRQ7.

CALIBRATION:

In data acquisition, it is important to constantly calibrate measurement device to maintain its accuracy. A calibration program, CAL711B.EXE is provided in the PCL-711B soft ware disk to assist calibration work. Equipment required to perform a satisfactory calibration is a 4 1/2 digit digital multi-meter. In addition, a voltage calibrator or a stable noise free d.c. voltage source that can be used in conjunction with the digital multi-meter is required.

VR Assignments

The PCL-711B has five on-board VR s, which allow making accurate calibration adjustments for the card's A/D and D/A functions. Each VR's location is indicated in figure (M-1). The function of each VR is listed below:

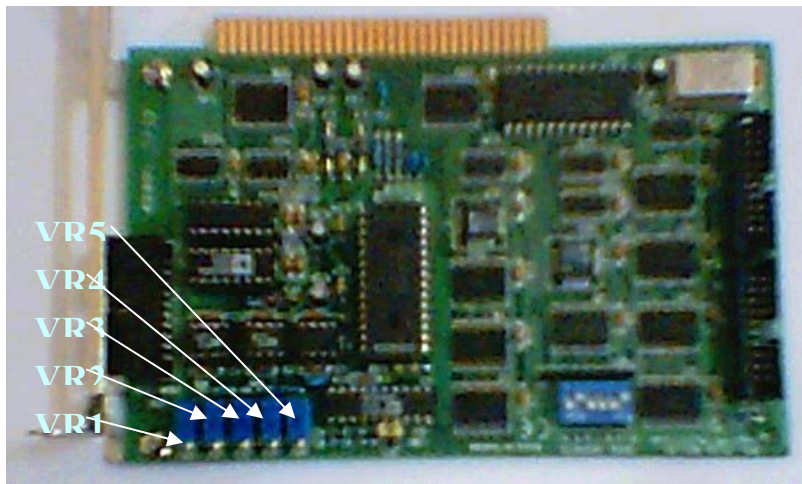
VR1	D/A full scale adjustment
VR2	D/A offset adjustment
VR3	A/D offset adjustment
VR4	A/D full-scale adjustment
VR5	Programmable amplifier offset adjustment

A/D Calibration

Because the PCL-711B supports. Versatile A/D input ranges, accurately calibrated result for certain A/D rang may still cause a small offset for the other ranges. It is suggested that you make a calibration again when you are going to use different A/D input range.

Calibration steps:

1. Short the A/D input of Channel 0 to AGND. Then, adjust the VR3 until the reading of the A/D conversion flickers between 2047 and 2048.
2. Apply a voltage with the full-scale value corresponding to the specific A/D input rang to A/D Channel 0. Then, adjust the VR4 until the reading of A/D conversion flickers between 4094 and 4095.



Variable resistance location in the card